SYK Meets Non-Hermiticity I: Emergent Replica Conformal Symmetry

Pengfei Zhang,[1,*] Shao-Kai Jian,[2,*] Chunxiao Liu,[3,†] and Xiao Chen[4,‡]

[1]*Institute for Quantum Information and Matter and Walter Burke Institute for Theoretical Physics, California Institute of Technology, Pasadena, CA 91125, USA*
[2]*Condensed Matter Theory Center and Joint Quantum Institute, Department of Physics, University of Maryland, College Park, MD 20742, USA*
[3]*Department of Physics, University of California Santa Barbara, Santa Barbara, CA 93106, USA*
[4]*Department of Physics, Boston College, Chestnut Hill, MA 02467, USA*

(Dated: April 12, 2021)

Recently, the steady states of non-unitary free fermion dynamics are found to exhibit novel critical phases with power-law squared correlations and a logarithmic subsystem entanglement. In this work, we theoretically understand the underlying physics by constructing solvable static/Brownian quadratic Sachdev-Ye-Kitaev chains with non-Hermitian dynamics. We find the action of the replicated system generally shows (one or infinite copies of) $O(2) \times O(2)$ symmetries, which is broken to $O(2)$ by the saddle-point solution. This leads to an emergent conformal field theory of the Goldstone modes. We derive their effective action and obtain the universal critical behaviors of squared correlators. Furthermore, the entanglement entropy of a subsystem A with length L_A corresponds to the energy of the half-vortex pair $S \sim \rho_s \log L_A$, where ρ_s is the stiffness of the Goldstone mode. We also discuss special limits where more than one Goldstone mode exists and comment on interaction effects.

Introduction. – Under unitary evolution, local quantum information of a generic closed many-body system goes through the process of scrambling and disperses into the entire system. It has long been known that such process is closely related to thermalization, in which the entanglement entropy of a small subsystem approaches thermal entropy with volume law scaling [1, 2]. Ever since then, systems that evade quantum thermalization have been of special interest. Several mechanisms have been proposed in an effort to realize such systems, including many-body localization [3, 4], prethermalization [5, 6] and non-unitary evolution.

Among these mechanisms, the non-unitary evolution is especially natural since all experimental systems are inevitably open [7]. In a unitary dynamics under repeated measurement, if we follow the *quantum trajectories*, the steady state is non-thermal and can exhibit entanglement phase transition from a volume law phase to an area law phase [8–25]. The underlying mechanism also applies to other non-unitary dynamics that host exotic non-thermal phases [26–31]. For instance, in free fermion non-unitary systems, it is shown that a stable critical phase exists, in which the entanglement entropy is logarithmic in the subsystem size and the correlation functions in the spatial direction exhibits power-law decay [25, 32–34]. While these results have been corroborated in numerous numerical simulations, concrete solvable models, in which the entanglement entropy and correlation function can be determined analytically, are still lacking, and will prove valuable in the understanding of the intimate relation between quantum thermalization and non-Hermiticity.

The Sachdev-Ye-Kitaev$_q$ (SYK$_q$) models [35–37] describe N randomly interacting Majorana fermions with infinite-range q-fermion interactions. It is found to be solvable in the large-N limit where the entanglement entropy and its quench dynamics can be studied [33, 38–45]. Based on the original SYK model, different generalizations have been constructed. In particular, SYK chains (i.e. coupled SYK dots) have been proposed to understand various dynamical problems in 1D [46–52]. In [53, 54], the authors further consider introducing the temporal randomness into the SYK model, where the static random interaction terms are replaced by Markovian random interactions. This is known as the Brownian SYK model.

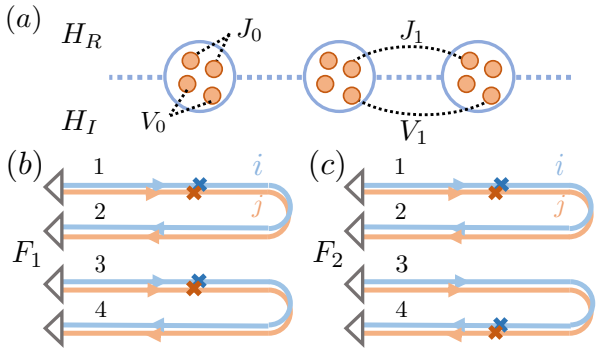

FIG. 1: (a). Schematics of the non-Hermitian SYK$_2$ chains studied in the work. The total Hamiltonian is given by $H = H_R - iH_I$ and the interaction can be either static or Brownian, (b/c). The path-integral contour for the squared correlator F_1/F_2. Here the triangles represent the contraction with the initial state $|\psi_0\rangle$. The crosses represent the insertion of Majorana operators.

In this work, combining ideas of non-Hermiticity and the SYK models, we construct a set of concrete non-Hermitian SYK$_2$ chains and derive the dynamical properties of the steady state in the large-N limit. By analyzing the saddle-point equation, we explicitly show that for generic values of the coupling parameters the replicated system exhibits a *replica conformal symmetry* due to the existence of Goldstone modes. We demonstrate that the Goldstone modes can be probed by the squared correlator which features the universal critical scaling. We then argue that the entanglement entropy for a subsystem A with length L_A corresponds to the energy of a half-vortex pair [25], given by $S \sim \rho_s \log L_A$, where ρ_s is the stiff-

ness of the Goldstone mode [55, 56]. We finally comment that when the interaction is added, the Goldstone mode acquires a mass, leading to a volume-law scaling in the entanglement entropy which can again be understood from a domain wall picture.

Model and Setup. – We consider non-Hermitian SYK$_2$ chains with Hamiltonian written in terms of

$$\begin{aligned} H_R &= \sum_{x,ij}\left[iJ_{ij}^{x,x+1}\chi_x^i\chi_{x+1}^j + i\tilde{J}_{ij}^x\chi_x^i\chi_x^j/2\right], \\ H_I &= \sum_{x,ij}\left[iV_{ij}^{x,x+1}\chi_x^i\chi_{x+1}^j + i\tilde{V}_{ij}^x\chi_x^i\chi_x^j/2\right]. \end{aligned} \tag{1}$$

Here $i = 1, 2...N$ labels the Majorana modes on each sites. The total Hamiltonian for the chain reads $H = H_R - iH_I$. Random hopping parameters $J_{ij}^{x,x+1}$, $\tilde{J}_{ij}^x$, $V_{ij}^{x,x+1}$, $\tilde{V}_{ij}^x$ are independent Gaussian variables with zero expectation value. We first focus on the case of static correlations and take their variances as

$$\begin{aligned} \overline{(J_{ij}^{x,x+1})^2} &= J_1^2/2N, \quad \overline{(\tilde{J}_{ij}^x)^2} = J_0^2/N, \\ \overline{(V_{ij}^{x,x+1})^2} &= V_1^2/2N, \quad \overline{(\tilde{V}_{ij}^x)^2} = V_0^2/N. \end{aligned} \tag{2}$$

The case of Brownian correlations will be considered later.

We aim to understand the steady states under the non-Hermitian dynamics. We consider preparing the system in some initial state $|\psi_0\rangle$. For a given disorder configuration, at time T, the system is in the state

$$|\psi(T)\rangle = e^{-iHT}|\psi_0\rangle / \sqrt{\langle\psi_0| e^{iH^\dagger T}e^{-iHT}|\psi_0\rangle}. \tag{3}$$

We are interested in understanding the emergence of the criticality in the non-unitary dynamics shown above [33]. A natural object to study is the Keldysh equal-time two-point function

$$\left\langle\chi_x^i\chi_0^j\right\rangle \equiv \lim_{T\to\infty}\frac{\langle\psi_0| e^{iH^\dagger T}e^{-iHT/2}\chi_x^i\chi_0^j e^{-iHT/2}|\psi_0\rangle}{\langle\psi_0| e^{iH^\dagger T}e^{-iHT}|\psi_0\rangle}$$

evaluated on the steady state. However, in random system, the disorder averaged $\overline{\left\langle\chi_x^i\chi_0^j\right\rangle}$ vanishes, and we should instead consider the disorder averaged squared correlators. We define two types of the squared correlators as

$$F_1 = \sum_{ij}\overline{\left\langle\chi_x^i\chi_0^j\right\rangle^2}/N, \qquad F_2 = \sum_{ij}\overline{\left|\left\langle\chi_x^i\chi_0^j\right\rangle\right|^2}/N.$$

These correlators measure the fluctuations of two-point functions over disorder realizations.

The computation of the correlation functions for disordered quantum systems generally requires the introduction of additional disorder replicas. However, for the SYK-like models in the large-N limit, the saddle point solution is diagonal in the disorder replicas [36, 57, 58]. Consequently, F_1 and F_2 can be represented as four-point functions on the replicated partition function in a single disorder replica:

$$\overline{Z^2} = \overline{(\langle\psi_0| e^{iH^\dagger t}e^{-iHt}|\psi_0\rangle)^2}. \tag{4}$$

In the path-integral formulation of $F_{1,2}$, there are four branches of the evolution contour, as shown in FIG. 1 (b-c). We label these four branches by 1-4 where the evolution is forward on $1, 3$ and backward on $2, 4$. Following the standard SYK derivation, the system is described by a bilocal G-Σ action [59], which can then be treated within the saddle-point approximation. The effective action that governs the fluctuations around the saddle point can be subsequently derived, which allows to determine the squared correlators analytically. Moreover, the entanglement calculation can be viewed as introducing defects on the boundary of the contour at time T. They excite the fluctuations with an energy increase equal to the entanglement entropy.

Saddle point and Symmetry. – We begin with analyzing the saddle-point equation. From now on, we keep the Majorana index i implicitly. For SYK-like models, the saddle-point equation is equivalent to the Schwinger-Dyson equation for $G_x^{ab}(t,t') \equiv \left\langle\chi_x^a(t)\chi_x^b(t')\right\rangle$ with $a, b \in \{1, 2, 3, 4\}$ labeling Majorana fields on different branches of the contour. Viewing G as a matrix in the branch and the time space, we have

$$\left[(-1)^{a+1}\delta^{ac}\partial_t - \Sigma_x^{ac}\right]\circ G_x^{cb} = I^{ab}. \tag{5}$$

For our static model, the self-energy Σ_x^{ac} reads

$$\Sigma_x^{ab} = (V_1^2 - (-1)^{a+b}J_1^2)\frac{G_{x+1}^{ab} + G_{x-1}^{ab}}{2} + (V_0^2 - (-1)^{a+b}J_0^2)G_x^{ab}, \tag{6}$$

this equation contains large symmetries which are rotations between the $1, 3$ or $2, 4$ branches. To see this, we define the Fourier transformation as $G_x^{ab}(\omega_1,\omega_2) \equiv \int dtdt'\, e^{i(\omega_1 t+\omega_2 t')}G_x^{ab}(t,t')$. The Schwinger-Dyson equation is then invariant under $G(\omega_1,\omega_2) \to O(\omega_1)G(\omega_1,\omega_2)O^T(-\omega_2)$, with $O(\omega) = \exp(-\gamma_{13}\theta_{13}^\omega - \gamma_{24}\theta_{24}^\omega)$, here $(\gamma_{cd})^{ab} = \delta_{ac}\delta_{bd} - \delta_{bc}\delta_{ad}$ is a 4×4 matrix in the branch space. Consequently, there are infinite copies of the $O(2)\times O(2)$ symmetry, labeled by the frequency ω. Similar symmetry appears when computing the spectral form factor [60]. We note that there is an additional time-reversal symmetry under $t \to -t$ and $G^{ab}(t,t') \to (-1)^{a+b}G^{5-a,5-b}(-t,-t')$ [61].

Now we present the solution of the saddle-point equation away from the boundary $t = 0$ or $t = T$. Assuming sufficiently large T, such that the system reaches the steady state and the Green's function becomes translationally invariant in both space and time directions $G_x^{ab}(t,t') = G_s^{ab}(t-t')$. Moreover, since the branches $1, 2$ decouple from the branches $3, 4$, we expect G_s^{ab} to be block diagonal with $G_s^{13} = G_s^{14} = G_s^{23} = G_s^{24} = 0$ and $G_s^{ab} = G_s^{a+2,b+2}$ for $a, b \in \{1, 2\}$ [62]. In the low-energy limit $|\omega| < \frac{2J^2}{\sqrt{J^2+V^2}}$, $G_s(\omega)$ reads

$$G_s^{11}(\omega) = \frac{i\omega}{2J^2}, \quad G_s^{12}(\omega) = -\frac{1}{2J^2}\sqrt{\frac{4J^4}{J^2+V^2} - \omega^2}, \tag{7}$$

together with $G_s^{22}(t) = -G_s^{11}(t)$ and $G_s^{21}(t) = -G_s^{12}(t)$. Here we have defined $J^2 \equiv J_0^2 + J_1^2$, $V^2 \equiv V_0^2 + V_1^2$. For $|\omega| > \frac{2J^2}{\sqrt{J^2+V^2}}$,

we instead have

$$G_s^{11}(\omega) = i\frac{\omega\left(1-\sqrt{1-\frac{4(J^2-V^2)}{\omega^2}}\right)}{2(J^2-V^2)}, \quad G_s^{12}(\omega)=0. \tag{8}$$

For each frequency $|\omega| < \frac{2J^2}{\sqrt{J^2+V^2}}$, the solutions (7) break the $O(2)\times O(2)$ symmetry but preserve the time-reversal symmetry. The solutions are only invariant under the symmetry transformation when $\theta_{13} = \theta_{24}$. We denote the residue symmetry group by $O(2)_+$, where the subscript represents the generator is $\gamma_{13}+\gamma_{24}$. The Goldstone mode lives in the coset space $O(2)\times O(2)/O(2)_+$ space and is given by $[G_s, \gamma_{13}-\gamma_{24}]$. In terms of the original bilocal fields, they correspond to $\delta G^{14}_{k=0}(\omega,-\omega) = \delta G^{23}_{k=0}(\omega,-\omega)$. Here we have defined the fluctuation of G fields as $\delta G^{ab}_k(\omega_1,\omega_2) \equiv \sum_x e^{-ikx}\delta G^{ab}_x(\omega_1,\omega_2)$. This suggests there should be a line of Goldstone modes labeled by frequency ω. Similar physics has also been observed in [25], where only a single $O(2)\times O(2)$ group exists [63].

Special limits exist in which the symmetry of the model is enlarged from $O(2)\times O(2)$. As explained in the supplementary material [59], when $J_1 = V_0 = 0$ or $J_0 = V_1 = 0$, rotations between 14 or 23 branches are also allowed, which leads to additional Goldstone modes at δG^{13} and δG^{14}. The detailed analysis also shows the mode is near $k=\pi$. However, as we will see later, such modes are not excited when considering a finite subsystem A, and thus does not contribute to the entanglement entropy. Nevertheless, as will be shown below, these modes can be probed by the squared correlators.

Effective action and Squared correlators. – We now consider fluctuations around the saddle-point solution (7). The effective action for fluctuations is given by expanding the G-Σ action around the low-energy saddle-point solution (7). Since we are interested on the low-energy limit, we focus on fluctuations involving two replicas $\{\delta G^{13}, \delta G^{14}, \delta G^{23}, \delta G^{24}\}$. These modes decouple from single-replica modes at the quadratic level. Using the permutation symmetry between two replicas, we combine them into symmetric and anti-symmetric components $\phi_\pm = (\phi^1_\pm, \phi^2_\pm) = \frac{1}{\sqrt{2}}(\delta G^{13} \pm \delta G^{24}, \delta G^{14} \pm \delta G^{23})$. For general coupling parameters, only the symmetric component ϕ_+ is expected to be gapless due to the existence of Goldstone mode.

Expanding the action for small k and ω, we find for the static model the effective action of $\phi_+(\omega_1,\omega_2)$ takes the form:

$$-I_{\rm eff}/N = \frac{1}{2}\int_{\omega_1\omega_2 k}\phi_+\begin{pmatrix} 2V^2 & \frac{i(J^2+V^2)^{3/2}}{2J^2}\Omega \\ -\frac{i(J^2+V^2)^{3/2}}{2J^2}\Omega & -\frac{J_1^2+V_1^2}{2}k^2 + \frac{(J^2+V^2)^2\Omega^2}{8J^4}\end{pmatrix}\phi_+. \tag{9}$$

Here we have defined $\Omega = \omega_1+\omega_2$. As we expect, there are a line of Goldstone modes at $\Omega = 0$ labeled by $\omega = (\omega_1-\omega_2)/2$. Since the solution (7) is only valid for $|\omega_i| < \frac{2J^2}{\sqrt{J^2+V^2}}$, the effective action (34) is only valid below this cutoff. The theory is a conformal field theory with dynamical exponent $z=1$, as observed in previous numerics for $J_0 = V_1 = 0$ [33]. It is also useful to reformulate the effective action using

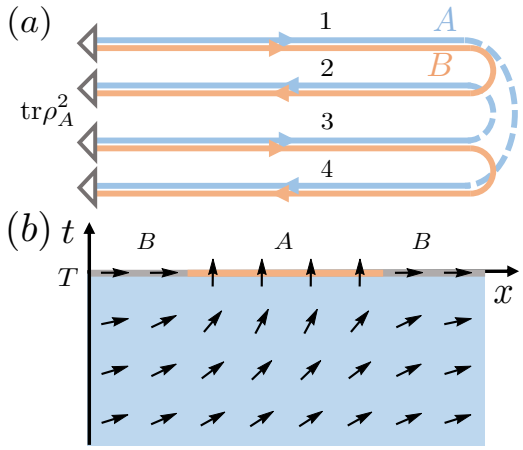

FIG. 2: A sketch for the calculation of the second Rényi entanglement entropy on the steady state. (a). The path-integral contour for the purity calculation. (b). The effective theory is an XY model on a half-infinite plane, with twisted boundary condition on the boundary $t=T$. The energy increase due to the creation of the half-vortex pair is equal to $S_A^{(2)}(\infty)$.

the fields $\theta^\omega(\Omega)$ in the coset space. Using $\delta G^{14} = \delta G^{23} = \sin\theta^\omega(\Omega) G_s^{12}(\omega) \approx \theta^\omega(\Omega) G_s^{12}(\omega)$ and integrating out ϕ^1_+, we find

$$\frac{I_{\rm eff}}{N} = \frac{1}{2}\int_{\omega\Omega k}\left(\frac{J_1^2+V_1^2}{J^2+V^2}k^2 + \frac{J^2+V^2}{4J^2V^2}\Omega^2\right)|\theta^\omega(\Omega,k)|^2. \tag{10}$$

The effective actions can also be inferred directly from the symmetry perspective: When $\Omega = k = 0$, the Goldstone modes δG^{14} cost zero energy while δG^{13} is gapped. Moreover, under the time-reversal symmetry, we have $\Omega \to -\Omega$ and $\phi_+ \to \sigma_z\phi_+$, which explains the off-diagonal terms which is linear in frequency. Finally, one can add quadratic terms in Ω and k allowed by symmetry, which leads to (34). Consequently, we expect the form of the effective action to be universal.

This leads to universal scaling for two-point functions of ϕ_+. In the language of the original fermions, they just correspond to squared correlators F_1 and F_2. Working out the Fourier transformation, we find the general scaling form

$$\begin{aligned} F_1 &= -\frac{\langle\phi_+\phi_+\rangle_{11}}{2} \sim \int e^{ikx}\frac{k^2}{\Omega^2+k^2} \sim 1/x^2, \\ F_2 &= \frac{\langle\phi_+\phi_+\rangle_{22}}{2} \sim \int e^{ikx}\frac{1}{\Omega^2+k^2} \sim \log x. \end{aligned} \tag{11}$$

Here we have omitted parameters that depending on the details of models. F_2 takes the same form as the correlation function of $2D$ massless bosons, while F_1 acquires taking additional derivatives. Nevertheless, the result of F_1 may be modified if additional Goldstone modes exist. Following the similar route, when there is an additional Goldstone mode at G^{13} and G^{24} (at momentum π) for special limits [59], we instead find $F_1 \sim (-1)^x \log x$.

Entanglement entropy. – We finally turn to the study of the second Rényi entanglement entropy of $|\psi(T)\rangle$. We choose

the subsystem A as first L_A sites of the chain, and its reduced density matrix $\rho_A(T) = \mathrm{tr}_B\,|\psi(T)\rangle\langle\psi(T)|$ is obtained by tracing out the remaining part B. We consider

$$\mathrm{tr}_A(\rho_A)^2 = \frac{\mathrm{tr}_A\left(\mathrm{tr}_B\, e^{-iHT}\,|\psi_0\rangle\langle\psi_0|\, e^{iH^\dagger T}\right)^2}{\left(\langle\psi_0|\, e^{iH^\dagger T} e^{-iHT}\,|\psi_0\rangle\right)^2} \equiv \frac{Z_2(T,A)}{Z^2(T)}, \quad (12)$$

and the second Rényi entropy is given by $S_A^{(2)}(T) = -\log \mathrm{tr}_A(\rho_A(T))^2$. Again, by assuming replica diagonality in the disorder replica space [36, 57, 58], one has

$$\overline{S_A^{(2)}(T)} \approx \log \overline{Z_2(T,A)} - \log \overline{Z_2(T,\emptyset)}. \quad (13)$$

The calculation of entanglement entropy can be mapped to the problem of computing the energy of half-vortex pair that emerges due to the special boundary conditions in the Rényi contour [25]. To illustrate this, we consider the evolution time T to be long enough and focus on the boundary at $t = T$. For subsystem A, the twisted boundary conditions connect branches 14 and 23 (see FIG. 2 (a)) which excites the Goldstone mode and effectively imposes a $\theta = \pi/2$ vortex on one boundary region of A and a $\theta = -\pi/2$ antivortex on the other. On the contrary, for subsystem B, the boundary condition favors $\theta = 0$ according to previous analysis. Together with the effective action (10), the problem maps to (infinite copies of) 2D XY models on a half-infinite plane with additional pinning fields creating half-vortex/antivortex on the boundaries. A sketch for this system is shown in FIG. 2 (b). The entanglement entropy (13) is equal to the energy of this half-vortex-antivortex pair with spatial separation L_A, which is known to be $S_A^{(2)} \propto \rho_s \log L_A$ [55, 56]; such a critical behavior is consistent with previous numerics [33]. Similarly, the mutual information is equal to (the opposite of) the interaction energy between two half-vortex pairs, which scales with $1/d^2$ where d is the distance between two subregions.

In the large-N limit, the XY model is at zero-temperature and we can directly apply the mean-field approximation. The stiffness (or the superfluid density) ρ_s is given by summing up contributions from different ω, which gives

$$\text{Static:} \quad S_A^{(2)} \propto \rho_s \log L_A \propto \frac{J}{V}\sqrt{\frac{J_1^2+V_1^2}{J^2+V^2}} N \log L_A. \quad (14)$$

Specifically, for large J_1/V_0 and $J_0 = V_1 = 0$ the result $J_1/V_0 \log L_A$ is consistent with the numerical observation in [33]. We further performed numerical simulation to verify that the scaling form (14) holds in a large parameter region with finite J and V; the numerical result for the stiffness ρ_s is shown in Fig. 3 (a) [64].

Brownian SYK. – Previously, there has been extensive studies on the Brownian circuit models [54, 65–70]. We can also generalize our SYK_2 chain to the Brownian case. Now, we treat $J_{ij}^{x,x+1}$, $\tilde{J}_{ij}^x$, $V_{ij}^{x,x+1}$, $\tilde{V}_{ij}^x$ as time-dependent variables with

$$\begin{aligned} \overline{J_{ij}^{x,x+1}(t)J_{ij}^{x,x+1}(0)} &= \frac{J_1}{2N}\delta(t), \quad \overline{\tilde{J}_{ij}^x(t)\tilde{J}_{ij}^x(0)} = \frac{J_0}{N}\delta(t), \\ \overline{V_{ij}^{x,x+1}(t)V_{ij}^{x,x+1}(0)} &= \frac{V_1}{2N}\delta(t), \quad \overline{\tilde{V}_{ij}^x(t)\tilde{V}_{ij}^x(0)} = \frac{V_0}{N}\delta(t). \end{aligned} \quad (15)$$

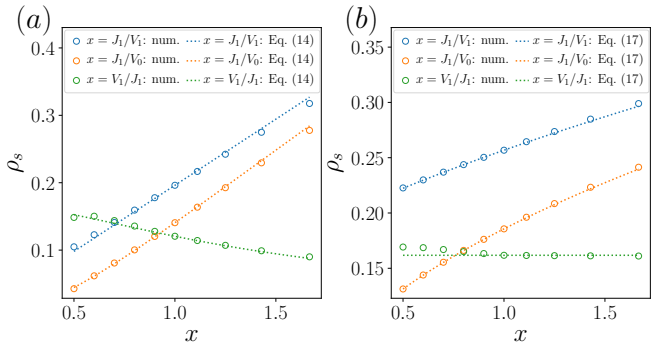

FIG. 3: Numerical result for the stiffness ρ_s in (a) the static SYK_2 chain and (b) the Brownian SYK_2 chain. The coupling parameters not mentioned in the plots are set to zero. The analytical expressions (14) and (17) are plotted for comparison.

Following the similar derivations as the static case, we find there is a single Goldstone mode with

$$\frac{I_{\text{eff}}}{N} = \frac{1}{2}\int_{\Omega k}\left(\frac{J_1+V_1}{4}k^2 + \frac{1}{4V}\Omega^2\right)|\theta(\Omega,k)|^2, \quad (16)$$

which takes a similar form as the static case due to the aforementioned time-reversal symmetry. Consequently, the universal scaling (11) still applies and ρ_s can be extracted from (16) to obtain

$$\text{Brownian:} \quad S_A^{(2)} \propto \rho_s \log L_A = \sqrt{\frac{J_1+V_1}{V}} N \log L_A. \quad (17)$$

Such a scaling is again verified numerically; the numerical value of the stiffness ρ_s is shown in Fig. 3 (b).

Discussions. – In this work, we study the non-unitary dynamics of the SYK_2 chains for both the static model and the Brownian model. In the replicated space, the system shows (copies) of the $O(2) \times O(2)$ symmetry, which is broken into $O(2)_+$ by the saddle-point solution. The system then obtains an emergent replica conformal symmetry from the fluctuation of Goldstone modes, leading to universal scaling of squared correlators. The entanglement entropy of a subsystem A can be understood as the energy of a half-vortex pair, which is logarithmic in subsystem size.

There are a lot of interesting extensions of this work. Firstly, our derivations can be directly applied to the higher dimensional SYK_2 lattices with little modification. For $2D$ lattices, the result is an XY model in $3D$. Choosing the A subsystem as a circle with perimeter L_A, the entanglement entropy then corresponds to the energy of a half-vortex ring, which is proportional to $\rho_S L_A \log L_A$. Secondly, we can add interactions to our model. As an example, consider we add an Brownian SYK_4 interaction term $\Delta H_R = \sum_{ijkl,x} g_{ijkl}^x(t)\chi_x^i\chi_x^j\chi_x^k\chi_x^l$. This leads to an additional self-energy term $-g\delta(t-t')(-1)^{a+b}G_x^{a,b}(t,t')^3$, which breaks the $O(2)\times O(2)$ symmetry explicitly. Consequently, the replicated system becomes gapped and there is no longer conformal symmetry. Furthermore, the entanglement entropy corresponds to the energy of a domain wall with length L_A, instead of a vortex

pair, leading to the volume law. Finally, it is also interesting to construct models with entanglement transitions. Such a model exists if we introduce two copies of the SYK chain and adding non-Hermiticity on the fermion parity operator between two copies. The system shows a transition between a critical phase and an area law phase when there is no interaction. After adding interactions, the system shows a second-order transition between a volume phase to an area law phase. These results will be presented in a separate paper [71].

Acknowledgment. We acknowledge helpful discussions with Ehud Altman. PZ acknowledges support from the Walter Burke Institute for Theoretical Physics at Caltech. SKJ is supported by the Simons Foundation via the It From Qubit Collaboration. CL is supported by the NSF CMMT program under Grants No. DMR-1818533. Use was made of computational facilities purchased with funds from the National Science Foundation (CNS-1725797) and administered by the Center for Scientific Computing (CSC). The CSC is supported by the California NanoSystems Institute and the Materials Research Science and Engineering Center (MRSEC; NSF DMR-1720256) at UC Santa Barbara.

* They contribute equally to this work.
† chunxiaoliu@ucsb.edu
‡ chenaad@bc.edu

[1] M. Srednicki, Phys. Rev. E **50**, 888 (1994).
[2] J. M. Deutsch, Phys. Rev. A **43**, 2046 (1991).
[3] R. Nandkishore and D. A. Huse, Annu. Rev. Condens. Matter Phys. **6**, 15 (2015).
[4] F. Alet and N. Laflorencie, Comptes Rendus Physique **19**, 498 (2018).
[5] D. Abanin, W. De Roeck, W. W. Ho, and F. Huveneers, Communications in Mathematical Physics **354**, 809 (2017).
[6] T. Kuwahara, T. Mori, and K. Saito, Annals of Physics **367**, 96 (2016).
[7] S. Banerjee, S. Banerjee, and Ahmad, *Open quantum systems* (Springer, 2018).
[8] X. Cao, A. Tilloy, and A. D. Luca, SciPost Phys. **7**, 24 (2019).
[9] Y. Li, X. Chen, and M. P. A. Fisher, Phys. Rev. B **98**, 205136 (2018).
[10] Y. Li, X. Chen, and M. P. A. Fisher, Phys. Rev. B **100**, 134306 (2019).
[11] B. Skinner, J. Ruhman, and A. Nahum, Phys. Rev. X **9**, 031009 (2019).
[12] A. Chan, R. M. Nandkishore, M. Pretko, and G. Smith, Phys. Rev. B **99**, 224307 (2019).
[13] Y. Bao, S. Choi, and E. Altman, Physical Review B **101** (2020), 10.1103/physrevb.101.104301.
[14] S. Choi, Y. Bao, X.-L. Qi, and E. Altman, Physical Review Letters **125** (2020), 10.1103/physrevlett.125.030505.
[15] M. J. Gullans and D. A. Huse, arXiv e-prints , arXiv:1905.05195 (2019), arXiv:1905.05195 [quant-ph] .
[16] M. J. Gullans and D. A. Huse, Phys. Rev. Lett. **125**, 070606 (2020).
[17] C.-M. Jian, Y.-Z. You, R. Vasseur, and A. W. W. Ludwig, Phys. Rev. B **101**, 104302 (2020).
[18] A. Zabalo, M. J. Gullans, J. H. Wilson, S. Gopalakrishnan, D. A. Huse, and J. H. Pixley, Phys. Rev. B **101**, 060301 (2020).
[19] Q. Tang and W. Zhu, Phys. Rev. Research **2**, 013022 (2020).
[20] M. Szyniszewski, A. Romito, and H. Schomerus, Phys. Rev. B **100**, 064204 (2019).
[21] L. Zhang, J. A. Reyes, S. Kourtis, C. Chamon, E. R. Mucciolo, and A. E. Ruckenstein, Physical Review B **101** (2020), 10.1103/physrevb.101.235104.
[22] S. Goto and I. Danshita, arXiv e-prints , arXiv:2001.03400 (2020), arXiv:2001.03400 [cond-mat.quant-gas] .
[23] S.-K. Jian, Z.-C. Yang, Z. Bi, and X. Chen, arXiv preprint arXiv:2101.04115 (2021).
[24] M. Buchhold, Y. Minoguchi, A. Altland, and S. Diehl, arXiv preprint arXiv:2102.08381 (2021).
[25] Y. Bao, S. Choi, and E. Altman, arXiv preprint arXiv:2102.09164 (2021).
[26] S. Sang and T. H. Hsieh, "Measurement protected quantum phases," (2020), arXiv:2004.09509 [cond-mat.stat-mech] .
[27] A. Lavasani, Y. Alavirad, and M. Barkeshli, Nature Physics **17**, 342–347 (2021).
[28] M. Ippoliti, T. Rakovszky, and V. Khemani, "Fractal, logarithmic and volume-law entangled non-thermal steady states via spacetime duality," (2021), arXiv:2103.06873 [quant-ph] .
[29] T.-C. Lu and T. Grover, "Entanglement transitions via spacetime rotation of quantum circuits," (2021), arXiv:2103.06356 [quant-ph] .
[30] C.-M. Jian, B. Bauer, A. Keselman, and A. W. W. Ludwig, "Criticality and entanglement in non-unitary quantum circuits and tensor networks of non-interacting fermions," (2020), arXiv:2012.04666 [cond-mat.stat-mech] .
[31] M. Ippoliti, M. J. Gullans, S. Gopalakrishnan, D. A. Huse, and V. Khemani, Physical Review X **11** (2021), 10.1103/physrevx.11.011030.
[32] X. Chen, Y. Li, M. P. A. Fisher, and A. Lucas, Physical Review Research **2** (2020), 10.1103/physrevresearch.2.033017.
[33] C. Liu, P. Zhang, and X. Chen, arXiv preprint arXiv:2008.11955 (2020).
[34] O. Alberton, M. Buchhold, and S. Diehl, "Trajectory dependent entanglement transition in a free fermion chain – from extended criticality to area law," (2020), arXiv:2005.09722 [cond-mat.stat-mech] .
[35] A. Kitaev, talk given at the KITP Program: entanglement in strongly-correlated quantum matter (2015).
[36] J. Maldacena and D. Stanford, Phys. Rev. D **94**, 106002 (2016).
[37] S. Sachdev and J. Ye, Phys. Rev. Lett. **70**, 3339 (1993).
[38] C. Liu, X. Chen, and L. Balents, Phys. Rev. B **97**, 245126 (2018).
[39] Y. Gu, A. Lucas, and X.-L. Qi, Journal of High Energy Physics **2017**, 120 (2017), arXiv:1708.00871 [hep-th] .
[40] Y. Huang and Y. Gu, Phys. Rev. D **100**, 041901 (2019).
[41] P. Zhang, C. Liu, and X. Chen, SciPost Phys. **8**, 94 (2020).
[42] A. Haldar, S. Bera, and S. Banerjee, arXiv e-prints , arXiv:2004.04751 (2020), arXiv:2004.04751 [cond-mat.str-el] .
[43] P. Zhang, Journal of High Energy Physics **2020**, 143 (2020).
[44] Y. Chen, X.-L. Qi, and P. Zhang, Journal of High Energy Physics **2020**, 121 (2020).
[45] J. Shao-Kai and B. Swingle, Journal of High Energy Physics **2021** (2021).
[46] Y. Gu, X.-L. Qi, and D. Stanford, Journal of High Energy Physics **2017**, 125 (2017), arXiv:1609.07832 [hep-th] .
[47] R. A. Davison, W. Fu, A. Georges, Y. Gu, K. Jensen, and S. Sachdev, Phys. Rev. B **95**, 155131 (2017).
[48] X. Chen, R. Fan, Y. Chen, H. Zhai, and P. Zhang, Phys. Rev.

Lett. **119**, 207603 (2017).
[49] X.-Y. Song, C.-M. Jian, and L. Balents, Phys. Rev. Lett. **119**, 216601 (2017).
[50] P. Zhang, Phys. Rev. B **96**, 205138 (2017).
[51] C.-M. Jian, Z. Bi, and C. Xu, Phys. Rev. B **96**, 115122 (2017).
[52] Y. Chen, H. Zhai, and P. Zhang, Journal of High Energy Physics **2017**, 150 (2017), arXiv:1705.09818 [hep-th] .
[53] P. Saad, S. H. Shenker, and D. Stanford, arXiv preprint arXiv:1806.06840 (2018).
[54] C. Sünderhauf, L. Piroli, X.-L. Qi, N. Schuch, and J. I. Cirac, Journal of High Energy Physics **2019**, 38 (2019), arXiv:1908.00775 [quant-ph] .
[55] C. J. Pethick and H. Smith, *Bose–Einstein condensation in dilute gases* (Cambridge university press, 2008).
[56] H. Zhai, *Ultracold Atomic Physics* (Cambridge University Press, 2021).
[57] A. Kitaev and S. J. Suh, Journal of High Energy Physics **2018**, 183 (2018), arXiv:1711.08467 [hep-th] .
[58] Y. Gu, A. Kitaev, S. Sachdev, and G. Tarnopolsky, Journal of High Energy Physics **2020**, 157 (2020), arXiv:1910.14099 [hep-th] .
[59] See supplementary material for: 1. The path-integral approach for the replicated SYK chains; 2. The derivation of the effective action for Goldstone modes; 3. Some special limits of the model.
[60] M. Winer, S.-K. Jian, and B. Swingle, Physical Review Letters **125**, 250602 (2020).
[61] Note that at the level of the Schwinger-Dyson equation, the phase introduced here is unnecessary. The choice is to make the symmetry not broken by the saddle-point solution.
[62] The block diagonal form is verified numerically.
[63] This is similar to the Brownian SYK_2 chain model.
[64] In the numerics, we take the initial state $|\psi_0\rangle$ to be the maximally entangled state between Majorana fermions with even and odd indices $c_x^i|\psi_0\rangle = 0$ where $c_x^i = \chi_x^{2i-1} + i\chi_x^{2i}$. The numerical details have been explained in previous works [33].
[65] N. Lashkari, D. Stanford, M. Hastings, T. Osborne, and P. Hayden, Journal of High Energy Physics **2013** (2013), 10.1007/jhep04(2013)022.
[66] T. Zhou and X. Chen, Physical Review E **99** (2019), 10.1103/physreve.99.052212.
[67] S. Xu and B. Swingle, Physical Review X **9** (2019), 10.1103/physrevx.9.031048.
[68] X. Chen and T. Zhou, Physical Review B **100** (2019), 10.1103/physrevb.100.064305.
[69] A. Lucas, arXiv e-prints , arXiv:1903.01468 (2019), arXiv:1903.01468 [cond-mat.str-el] .
[70] L. Piroli, C. Sünderhauf, and X.-L. Qi, Journal of High Energy Physics **2020** (2020), 10.1007/jhep04(2020)063.
[71] Shao-Kai Jian, et. al., to appear (2021).

Supplementary Material: SYK Meets Non-Hermiticity I: Emergent Replica Conformal Symmetry

In this supplementary material, we present: 1. The path-integral representation of the replicated system, 2. The derivation of the effective action, and 3. Discussions on spectial limits of the model.

THE PATH-INTEGRAL REPRESENTATION OF THE REPLICATED SYSTEM

As explained in the main text, we focus on the path-integral representation of the replicated system. We begin with the static case. The time evolution of a density matrix ρ is

$$\rho(t) = e^{-iHt}\rho e^{iH^\dagger t}, \tag{18}$$

and it does not preserve the normalization. To evaluate $\rho(t)$ using path integral, one needs two contours similar to the Keldysh contour. Denoted by 1 and 2 for forward and backward evolution, the action on these two contours schematically is

$$-I = \int dt\left(\frac{1}{2}\chi_x^a(-1)^a\partial_t\chi_x^a + (-1)^a\left(J^{x,x+1}\chi_x^a\chi_{x+1}^a + J^x\chi_x^a\chi_x^a\right) + i\left(V^{x,x+1}\chi_x^a\chi_{x+1}^a + V^x\chi_x^a\chi_x^a\right)\right), \tag{19}$$

where $a = 1, 2$ denotes two contours, and the superscript for Majorana species on each site is suppressed. After introducing two replicas, we aim to compute

$$\overline{Z^2} = \overline{(\langle\psi_0|\, e^{iH^\dagger T}e^{-iHT}\,|\psi_0\rangle)^2}. \tag{20}$$

This basically doubles the action on the Keldysh contour. Namely, it requires four contours denoted by 1, 2, 3, 4. The effective action on these four contours after integrating out disorder is

$$\begin{aligned}-\frac{I}{N} = \quad & \sum_x \frac{1}{2}\mathrm{Tr}\log\left((-1)^{a+1}\delta^{ab}\partial_t - \Sigma_x^{ab}\right) + \int\Big[-\frac{1}{2}\Sigma_x^{ab}G_x^{ab} \\ & +\frac{1}{4}[V_0^2(G_x^{ab})^2 + V_1^2G_x^{ab}G_{x+1}^{ab}] - \frac{(-1)^{a+b}}{4}[J_0^2(G_x^{ab})^2 + J_1^2G_x^{ab}G_{x+1}^{ab}]\Big],\end{aligned} \tag{21}$$

where G^{ab} and Σ^{ab} are the bilocal fields characterizing the two point function of Mojarana fermions at a and b contours. As a result, the saddle point equation is

$$[G_x^{-1}]^{ab} = (-1)^{a+1}\delta^{ab}\partial_t - \Sigma_x^{ab}, \tag{22}$$

$$\Sigma_x^{ab} = [V_0^2 - (-1)^{a+b}J_0^2]G_x^{ab} + [V_1^2 - (-1)^{a+b}J_1^2]\frac{G_{x-1}^{ab} + G_{x+1}^{ab}}{2}. \tag{23}$$

For the Brownian case, precisely, the Hamiltonian is time-dependent, and we keep the time-ordering in (18) and (20) implicit. Following similar steps, the result reads

$$-\frac{I}{N} = \sum_x \frac{1}{2}\mathrm{Tr}\log\left((-1)^{a+1}\delta^{ab}\partial_t - \Sigma_x^{ab}\right) + \int\Big[-\frac{1}{2}\Sigma_x^{ab}G_x^{ab} \tag{24}$$

$$+\frac{\delta}{4}[V_0(G_x^{ab})^2 + V_1G_x^{ab}G_{x+1}^{ab}] - \frac{(-1)^{a+b}\delta}{4}[J_0(G_x^{ab})^2 + J_1G_x^{ab}G_{x+1}^{ab}]\Big], \tag{25}$$

Here the main difference compared to the static case is the appearance of the additional $\delta = \delta(t_1 - t_2)$ due to the lack of correlation in the time direction. The gives

$$[G_x^{-1}]^{ab} = (-1)^{a+1}\delta^{ab}\partial_t - \Sigma_x^{ab}, \tag{26}$$

$$\Sigma_x^{ab} = \delta[V_0 - (-1)^{a+b}J_0]G_x^{ab} + \delta[V_1 - (-1)^{a+b}J_1]\frac{G_{x-1}^{ab} + G_{x+1}^{ab}}{2}. \tag{27}$$

Different from the static case, now there is only a single $O(2) \times O(2)$ symmetry, given by the transformation $G(t,t') \to OG(t,t')O^T$ with $O = \exp(-c_{13}\theta_{13} - c_{24}\theta_{24})$. The saddle-point solution takes a simpler form

$$G_s^{11}(\omega) = \frac{i\omega}{\omega^2 + \Gamma^2/4}, \quad G_s^{12}(\omega) = -\frac{\Gamma/2}{\omega^2 + \Gamma^2/4}. \tag{28}$$

Here $\Gamma = V + J = V_0 + V_1 + J_0 + J_1$ is the quasi-particle decay rate. The solution also breaks the symmetry down to $O(2)_+$, leading to a single Goldstone mode.

THE DERIVATION OF THE EFFECTIVE ACTION

The effective action is given by expanding the $G-\Sigma$ action (21) or (24) around the saddle-point solution. In this section, we give a detailed derivation for the effective actions.

The static model

we consider the saddle point fluctuations,

$$\Sigma_x(\omega_1,\omega_2)=\Sigma_s(\omega_1)2\pi\delta(\omega_1+\omega_2)+\delta\Sigma_x(\omega_1,\omega_2). \tag{29}$$

and similar for G, where we have used the convention $\Sigma(t_1,t_2)=\int\frac{d\omega_1}{2\pi}\frac{d\omega_2}{2\pi}\Sigma(\omega_1,\omega_2)e^{-i\omega_1 t_1-i\omega_2 t_2}$ for Fourier transformation. The trace log term in (21) gives rise to [as the first line in (21) does not depend on lattice site, we suppress lattice index x until we move on to evaluate the second line in (21)]

$$-\frac{1}{4}\int_{\omega_1,\omega_2}\delta\Sigma^{ab}(\omega_1,\omega_2)G_s^{da}(\omega_1)G_s^{bc}(-\omega_2)\delta\Sigma^{cd}(-\omega_2,-\omega_1). \tag{30}$$

where $\int_\omega\equiv\int\frac{d\omega}{2\pi}$ We will be interested in the correlation between 1, 2 and 3, 4, so we focus on these correlation functions. Assuming the symmetry $\Sigma^{ab}(t_1,t_2)=-\Sigma^{ba}(t_2,t_1)$, we can bring the kernel into

$$\int_{\omega_1,\omega_2}\frac{1}{8J^4}\hat{\sigma}(\omega_1,\omega_2)\begin{pmatrix}\omega_1\omega_2 & -f(\omega_1)f(\omega_2) & -i\omega_1 f(\omega_2) & -i\omega_2 f(\omega_1)\\ -f(\omega_1)f(\omega_2) & \omega_1\omega_2 & -i\omega_2 f(\omega_1) & -i\omega_1 f(\omega_2)\\ i\omega_1 f(\omega_2) & i\omega_2 f(\omega_1) & -\omega_1\omega_2 & f(\omega_1)f(\omega_2)\\ i\omega_2 f(\omega_1) & i\omega_1 f(\omega_2) & f(\omega_1)f(\omega_2) & -\omega_1\omega_2\end{pmatrix}\hat{\sigma}(-\omega_1,-\omega_2), \tag{31}$$

where we have defined $\hat{\sigma}\equiv(\delta\Sigma^{13},\delta\Sigma^{24},\delta\Sigma^{14},\delta\Sigma^{23})$ and $f(\omega)\equiv\sqrt{\frac{4J^4}{J^2+V^2}-\omega^2}$.

If one notices the coupling term $-\frac{1}{2}\int\Sigma^{ab}G^{ab}$ in (21), then it is a straightforward task to integrate out $\hat{\sigma}$ field, and the resultant action reads

$$\begin{aligned}&\int_{\omega_1,\omega_2}\frac{(J^2+V^2)^2}{8J^4}\\ &\times\hat{g}_k(\omega_1,\omega_2)\begin{pmatrix}-\omega_1\omega_2 & f(\omega_1)f(\omega_2) & i\omega_1 f(\omega_2) & i\omega_2 f(\omega_1)\\ f(\omega_1)f(\omega_2) & -\omega_1\omega_2 & i\omega_2 f(\omega_1) & i\omega_1 f(\omega_2)\\ -i\omega_1 f(\omega_2) & -i\omega_2 f(\omega_1) & \omega_1\omega_2 & -f(\omega_1)f(\omega_2)\\ -i\omega_2 f(\omega_1) & -i\omega_1 f(\omega_2) & -f(\omega_1)f(\omega_2) & \omega_1\omega_2\end{pmatrix}\hat{g}_{-k}(-\omega_1,-\omega_2),\end{aligned} \tag{32}$$

where $\hat{g}_k\equiv(\delta G_k^{13},\delta G_k^{24},\delta G_k^{14},\delta G_k^{23})$. We restore the lattice index by going to the momentum space using $g_k\equiv\frac{1}{\sqrt{L}}\sum_x g_x e^{-ikx}$ with L the number of sites.

The second line in (21) is simple, and leads to

$$\int_{\omega_1,\omega_2}\frac{1}{2}\hat{g}_k(\omega_1,\omega_2)\begin{pmatrix}V_k^2-J_k^2 & 0 & 0 & 0\\ 0 & V_k^2-J_k^2 & 0 & 0\\ 0 & 0 & V_k^2+J_k^2 & 0\\ 0 & 0 & 0 & V_k^2+J_k^2\end{pmatrix}\hat{g}_{-k}(-\omega_1,-\omega_2). \tag{33}$$

So the effective action is given by the sum of (32) and (33).

The fields δG^{14} and δG^{23} are related to a Goldstone mode. More precisely, $\delta G^{14}+\delta G^{23}$ is the Goldstone mode, so they are gapless at zero frequency and momentum. Expanding the effetive action near zero frequency and keeping the leading term, it reads

$$\begin{aligned}\frac{-I_{\text{eff}}}{N}=&\frac{1}{2}\int_{\omega_1,\omega_2}\hat{\phi}_+(\omega_1,\omega_2)\begin{pmatrix}J^2-J_k^2+V^2+V_k^2-\frac{(J^2+V^2)^2(\omega_1+\omega_2)^2}{8J^4} & \frac{i(J^2+V^2)^{3/2}}{2J^2}(\omega_1+\omega_2)\\ \frac{-i(J^2+V^2)^{3/2}}{2J^2}(\omega_1+\omega_2) & -J^2+J_k^2-V^2+V_k^2+\frac{(J^2+V^2)^2(\omega_1+\omega_2)^2}{8J^4}\end{pmatrix}\hat{\phi}_+(-\omega_1,-\omega_2)\\ &+\hat{\phi}_-(\omega_1,\omega_2)\begin{pmatrix}-J^2-J_k^2-V^2+V_k^2+\frac{(J^2+V^2)^2(\omega_1-\omega_2)^2}{8J^4} & \frac{i(J^2+V^2)^{3/2}}{2J^2}(\omega_1-\omega_2)\\ \frac{-i(J^2+V^2)^{3/2}}{2J^2}(\omega_1-\omega_2) & J^2+J_k^2+V^2+V_k^2-\frac{(J^2+V^2)^2(\omega_1-\omega_2)^2}{8J^4}\end{pmatrix}\hat{\phi}_-(-\omega_1,-\omega_2),\end{aligned} \tag{34}$$

where we make the symmetrization and antisymmetrization of the fields $\hat{\phi}_\pm = \frac{1}{\sqrt{2}}(\delta G^{13} \pm \delta G^{24}, \delta G^{14} \pm \delta G^{23})$, like the conventional Kelydsh rotation. And remember $J_k^2 = J_0^2 + J_1^2 \cos k$, $V_k^2 = V_0^2 + V_1^2 \cos k$. Only keeping the $\hat{\phi}_+$ part and expand each elements to the leading order in small k and ω, we get the effective action presented in the main text.

The Brownian model

Now we consider saddle-point fluctuations,

$$\Sigma(t_1, t_2) = \Sigma_s(t_1, t_2) + \delta\Sigma(t_1)\delta(t_{12}), \quad G(t_1, t_2) = G_s(t_1, t_2) + \delta G(t_1, t_2). \tag{35}$$

We first evaluate the Tr log term and then the interaction terms. Expanding the Tr log term into second order, we arrive at

$$-\frac{1}{4}\int_{\omega,\Omega} \mathrm{Tr}\left[G_s(\omega+\Omega)\delta\Sigma(\Omega)G_s(\omega)\delta\Sigma(-\Omega)\right] = \frac{1}{2}\int_\Omega \sigma^T(\Omega)\mathcal{M}\sigma(-\Omega), \tag{36}$$

where $\int_\Omega \equiv \int \frac{d\Omega}{2\pi}$, and we have used the Fourier transform $\delta\Sigma(\Omega) = \int dt \delta\Sigma(t) e^{i\Omega t}$. In evaluating the kernel, we have used the symmetry of bilocal field $\Sigma^{ab}(t_1, t_2) = -\Sigma^{ba}(t_2, t_1)$, so there are four independent diagonal fields and six independent off-diagonal fields. The full kernel implies that (a) off-diagonal fields decouple from diagonal field and (b) four out of six independent off-diagonal fields have nontrivial interactions. We denote these four nontrivial off-diagonal fields to be $\sigma = \left(\delta\Sigma^{13}, \delta\Sigma^{24}, \delta\Sigma^{14}, \delta\Sigma^{32}\right)^T$, and the corresponding kernel reads

$$\mathcal{M} = \frac{\Gamma}{2(\Omega^2+\Gamma^2)}\begin{pmatrix} -1 & -1 & -i & i \\ -1 & -1 & -i & i \\ i & i & 1 & -1 \\ -i & -i & -1 & 1 \end{pmatrix}. \tag{37}$$

It is easy to check that the kernel has two zero modes, and we can make redefinition of the fields

$$\varphi(-\Omega) = U\sigma(-\Omega), \quad U = \frac{1}{\sqrt{2}}\begin{pmatrix} 1 & 1 & 0 & 0 \\ 0 & 0 & -1 & 1 \\ -1 & 1 & 0 & 0 \\ 0 & 0 & 1 & 1 \end{pmatrix}, \tag{38}$$

such that the last two fields are zero modes and the quadratic action for the first two fields are (we use φ to denote the first two fields in the following)

$$\frac{1}{2}\int_\Omega \varphi^T(\Omega)\mathcal{M}_U\varphi(-\Omega), \quad \mathcal{M}_U = U\mathcal{M}U^\dagger = \begin{pmatrix} -\frac{\Gamma}{\Omega^2+\Gamma^2} & \frac{i\Omega}{\Omega^2+\Gamma^2} \\ -\frac{i\Omega}{\Omega^2+\Gamma^2} & -\frac{\Gamma}{\Omega^2+\Gamma^2} \end{pmatrix}. \tag{39}$$

Now we are ready to integrate out φ fields. For the two zero modes, because they couple linearly to δG fields in the action (24), integrating them out leads to two constraints.

$$\delta G^{13}(t,t) = \delta G^{24}(t,t), \quad \delta G^{14}(t,t) = -\delta G^{32}(t,t). \tag{40}$$

For notational simplicity, we introduce another fields

$$\phi_1(\Omega) = \sqrt{2}\int dt \delta G^{13}(t,t) e^{i\Omega t}, \tag{41}$$

$$\phi_2(\Omega) = -\sqrt{2}\int dt \delta G^{14}(t,t) e^{i\Omega t}. \tag{42}$$

In terms of these field of interest φ_i, ϕ_i, $i = 1, 2$, the quadratic action reads

$$-\frac{I_{eff}}{N} = 12\int_\Omega \left(\frac{1}{2}\varphi_x^T(\Omega)\mathcal{M}_U\varphi_x(-\Omega) - \frac{\sqrt{2}}{2}\left[\phi_x(\Omega)\varphi_x(-\Omega) + \varphi_x(\Omega)\phi_x(-\Omega)\right]\right) \tag{43}$$

$$+ \int_t \left(V_k(\phi_{1,k}\phi_{1,-k} + \phi_{2,k}\phi_{2,-k}) - J_k(\phi_{1,k}\phi_{1,-k} - \phi_{2,k}\phi_{2,-k})\right). \tag{44}$$

where we restore the space index and make Fourier transform to momentum space in the second line, $\phi_x = \frac{1}{\sqrt{L}}\sum_k \phi_k e^{ikx}$, L is the number of the site of the chain. And we also define $J_k = J_0 + J_1\cos k$, $V_k = V_0 + V_1\cos k$, and one should distinguish it from the case of regular SYK_2 model. It is then straightforward to integrate out φ field to have

$$-\frac{I_{eff}}{N} = \frac{1}{2}\sum_k \int_\Omega \phi_k(\Omega)\begin{pmatrix} J - J_k + V + V_k & -i\Omega \\ i\Omega & -J + J_k - V + V_k \end{pmatrix}\phi_{-k}(-\Omega). \tag{45}$$

Expanding each elements to the leading order in small k and ω, we get

$$-\frac{I_{\text{eff}}}{N} = \frac{1}{2}\int_{\Omega k} \phi_k(\Omega)\begin{pmatrix} 2V & i\Omega \\ -i\Omega & -(J_1 + V_1)k^2/2 \end{pmatrix}\phi_k(\Omega). \tag{46}$$

In terms of the coset space variable $\theta(\Omega)$, this becomes the effective action presented in the main text.

Relation to the entanglement entropy

Here we explain the boundary condition for θ when computing the entanglement entropy. As discussed in the main text, the entanglement entropy corresponds to

$$e^{-S_A^{(2)}} = \lim_{T\to\infty}\text{tr}_A\left(\text{tr}_B(e^{-iHT}|\psi_0\rangle\langle\psi_0|e^{iH^\dagger T})\text{tr}_B(e^{-iHT}|\psi_0\rangle\langle\psi_0|e^{iH^\dagger T})\right). \tag{47}$$

In other words, for sites in the subsystem B, the boundary condition connects the forward and the backward evolution in the same replica which favors $G^{12} \neq 0$ and $G^{14} = 0$, while for sites in the subsystem A, the boundary condition connects the forward and the backward evolution in different replicas which favors $G^{12} = 0$ and $G^{14} \neq 0$. This directly corresponds to the excitation of Goldstone modes. More explicitly, if we work out the low-energy manifold

$$G_x(t) = \begin{pmatrix} G_s^{11} & \cos(\theta)G_s^{12} & 0 & \sin(\theta)G_s^{12} \\ -\cos(\theta)G_s^{12} & -G_s^{11} & \sin(\theta)G_s^{12} & 0 \\ 0 & -\sin(\theta)G_s^{12} & G_s^{11} & \cos(\theta)G_s^{12} \\ -\sin(\theta)G_s^{12} & 0 & -\cos(\theta)G_s^{12} & -G_s^{11} \end{pmatrix}. \tag{48}$$

Then in B/A subsystem, the boundary condition favors $\theta = 0$ or $\pi/2$. Computing the entropy corresponds to the calculation of the energy of two half-vortexes with opposite charge.

DISCUSSIONS ON SPECIAL LIMITS OF THE MODEL

As mentioned in the main text, in special limits, the symmetry of the system can be larger and additional Goldstone modes appear. In this section, we give a detailed discussions on these cases. We take the static case as an example, and finally comment on the Brownian case.

For the saddle-point equation (22), we consider:

1. In special cases the symmetry of the equation can be larger than $O(2)\oplus O(2)$ (for each frequency ω). For example, when we have purely Hermitian evolution with $V_0 = V_1 = 0$, we can define $\tilde{G}^{ab} = (-1)^a\tilde{G}^{ab}$. The self-consistent equation then reads

$$\begin{aligned} &i\omega_1\tilde{G}_x^{ac}(\omega_1,-\omega_2) - \int\frac{d\omega_3}{2\pi}\tilde{\Sigma}_x^{ab}(\omega_1,-\omega_3)\tilde{G}_x^{bc}(\omega_3,-\omega_2) = I^{ac}\delta(\omega_1-\omega_2), \\ &\tilde{\Sigma}_x^{ab}(\omega_1,\omega_3) = -J_1^2\frac{\tilde{G}_{x+1}^{ab}(\omega_1,\omega_3)+\tilde{G}_{x-1}^{ab}(\omega_1,\omega_3)}{2} - J_0^2\tilde{G}_x^{ab}(\omega_1,\omega_3). \end{aligned} \tag{49}$$

   The equation now becomes $O(4)$ symmetric: $\tilde{G}_x^{ac}(\omega_1,\omega_2) \to O(\omega_1)\tilde{G}_x^{ac}(\omega_1,\omega_2)O^T(-\omega_2)$ with arbitrary $O(4)$ matrices $O(\omega)$. The effective action now leads to diffusive behavior

$$\left\langle\delta G^{13}\delta G^{13}\right\rangle = -\left\langle\delta G^{24}\delta G^{24}\right\rangle \sim \frac{1}{\Omega^2+k^4}. \tag{50}$$

   where we have dropped non-universal coefficients.

2. There is additional symmetry between the forward and the backward evolution if $J_0 = 0$ and $V_1 = 0$. The reason is that if we consider two evolutions and neglect their boundary conditions

$$e^{-iHT}e^{iH^\dagger T} = e^{-iH_R T - H_I T}e^{iH_R T - H_I T} \tag{51}$$

If we define $\chi'_x = \chi_x(-1)^x$, we find $H_R \to -H_R$ with H_I unchanged. Consequently, There is an additional Goldstone mode with momentum π. The mode appears at $G^{13}_{k=\pi}(\omega,\omega)$ and $G^{24}_{k=\pi}(\omega,\omega)$. Explicitly, we have

$$\left\langle \delta G^{13}\delta G^{13}\right\rangle = \frac{1}{\omega^2 + (k-\pi)^2}. \tag{52}$$

3. Similar modes exists when we instead have $V_0 = 0$ and $J_1 = 0$. The idea is again to perform the transformation $\tilde{G}^{a,c} = (-1)^a \tilde{G}^{a,c}$. The self-energy becomes:

$$\tilde{\Sigma}^{ab}_x(\omega_1,\omega_3) = V_1^2(-1)^{a+b}\frac{\tilde{G}^{ab}_{x+1}(\omega_1,\omega_3) + \tilde{G}^{ab}_{x-1}(\omega_1,\omega_3)}{2} - J_0^2\tilde{G}^{ab}_x(\omega_1,\omega_3) \tag{53}$$

Back to the evolution operator language, this corresponds to the self-consistent equation of

$$e^{-iH_R T - H_I T}e^{-iH_R T + H_I T}e^{-iH_R T - H_I T}e^{-iH_R T + H_I T} \tag{54}$$

Here we neglect boundary conditions. Now if we perform a momentum shift by $\chi'_x = \chi_x(-1)^x$ for $e^{-iH_R T + H_I T}$ contours, then the path-integral show $O(4)$ symmetry, and again we have modes on $G^{13}_{k=\pi}(\omega,-\omega)$ and $G^{24}_{k=\pi}(\omega,-\omega)$. Note that compared to the previous case, the frequency for the modes are different. This leads to

$$\left\langle \delta G^{13}\delta G^{13}\right\rangle = \frac{1}{\Omega^2 + (k-\pi)^2}. \tag{55}$$

4. The purely imaginary evolution with $J_0 = J_1 = 0$ is also special. On the one hand, both contours are symmetric and there should be $O(4)$ symmetry. However, in this case we have $G^{12} \equiv 0$ and there should be no symmetry breaking and thus no Goldstone modes. Calculation gives

$$\left\langle \delta G^{13}\delta G^{13}\right\rangle \sim \frac{\Theta(\omega_1\omega_2)}{k^2 + |\Omega|} \qquad \left\langle \delta G^{13}\delta G^{13}\right\rangle \sim \frac{\Theta(-\omega_1\omega_2)}{k^2 + |\omega|}. \tag{56}$$

For the Brownian model, similar analysis shows for $V_0 = 0$ and $J_1 = 0$, there is a similar Goldstone mode at G^{13} and G^{24}. However, when $V_1 = 0$ and $J_0 = 0$, the mode does not appear due to the lack of correlation in the time domain. Furthermore, different from the static model, G^{12} is non-trivial even under the purely imaginary evolution. Consequently, the result is the same as the general case, as mentioned in the main text.